remote sensing

MDPI

Technical Note

Sparse Inversion for the Iterative Marchenko Scheme of Irregularly Sampled Data

Jingwen Zeng and Liguo Han *

College of Geo-Exploration Science and Technology, Jilin University, Changchun 130026, China
* Correspondence: hanliguo@jlu.edu.cn

Abstract: The Marchenko method is a data-driven way that makes it possible to calculate Green's functions from virtual points in the subsurface using the reflection data at the surface and requiring only a macro velocity model. This method requires collocated sources and receivers. However, in practice, irregular sampling of sources or receivers will cause gaps and distortions in the obtained focusing functions and Green's functions. To solve this problem, this paper proposes to integrate a sparse inversion into the iterative Marchenko scheme. Specifically, we add sparsity constraints to the Marchenko equations and apply the sparse inversion during the iterative process. To reduce the strict requirements on acquisition geometries, our work deals with the situation in which the sources are subsampled where the integrations are carried out over the receivers, while the existing point spread function method solves the situation where the receivers are subsampled. We make a step to handle both situations at the same time by integrating this method with our work because of the same iterative framework. Our new method is applied to a two-dimensional numerical example with irregularly sampled data. The result shows that it can effectively fill gaps in the obtained focusing functions and Green's functions in the Marchenko method.

Keywords: Marchenko method; irregular sampling; focusing function; Green's function; sparse inversion

Citation: Zeng, J.; Han, L. Sparse Inversion for the Iterative Marchenko Scheme of Irregularly Sampled Data. *Remote Sens.* **2023**, *15*, 322. https://doi.org/10.3390/rs15020322

Academic Editors: Ru-Shan Wu, Benfeng Wang and Jingrui Luo

Received: 29 November 2022
Revised: 3 January 2023
Accepted: 3 January 2023
Published: 5 January 2023

1. Introduction

The Marchenko method is a data-driven method. It can bring Green's functions from focal points from the subsurface to the surface, requiring only the reflection response measured at the surface and direct arrivals from focal points to the surface [1–3]. Green's functions are the waves that reach a receiver position due to the firing of an impulsive source [4]. The obtained response does not have any internal multiples related to the overburden. The term "Marchenko" comes from the name of Vladimir Alexandrovich Marchenko, who studied the inverse scattering theory and deduced an equation to estimate Green's functions in one-dimensional quantum mechanics. Marchenko equations have long been used by mathematical physicists as the basis of one-dimensional inverse scattering theory [5–10]. In 2012, Broggini and Snieder introduced the Marchenko equation to the field of geophysics [11].

Similarly, Bakulin and Calvert proposed the virtual source method based on seismic interferometry [12]. This method can also retrieve Green's function. However, there should be a physical receiver as the virtual source in the medium that requires illumination from both above and below [13]. However, in practice, illumination generally appears only from the top, which means that the retrieved Green's function contains false multiples [14]. In contrast, the Marchenko method does not require a physical receiver inside the medium, and illuminating from one side is sufficient. In a one-dimensional medium, Green's functions between the virtual source in the medium and the receiver at the surface can be retrieved from the reflection response at the surface. Wapenaar et al. extended their work to 2D and 3D media [15]. Wapenaar and da Costa Filho et al. extended the method to elastic media [16,17]. Singh et al. discussed free surface multiples in this method [18]. Slob made

this method applicable to dissipative acoustic media [19]. The Marchenko method has been used for subsurface imaging without internal multiples [20–22] and internal multiple elimination [23,24].

However, there are some challenges related to the Marchenko method. This method requires collocated sources and receivers, low noise, no attenuation effect, and prior knowledge of the source signal. These requirements limit the wide application of the Marchenko method. This paper discusses the problem of strict acquisition geometry. For now, various ways are being sought to relax this limitation. Ravasi deduced the Rayleigh Marchenko equation so that the source could be placed at any position relative to the receiver [25]. Peng and Vasconcelos studied the subsampling and aperture-limiting effects in the Marchenko method [26]. Wapenaar and IJsseldijk rewrote the Marchenko equations considering the case of imperfect receiver sampling where the integrations were over receivers. They used a point spread function and multi-dimensional deconvolution for inversion to restore the distorted focusing functions and Green's functions [27]. Then this new representation of Marchenko equations was integrated into the iterative Marchenko scheme [28]. On the other side, Haindl et al. considered the case in which the sources are subsampled, proposing a sparse inversion method to compensate for the irregularity of the source [29].

In this paper, we focus on the situation where irregular sampling and integrating are over different dimensions, as Haindl et al. did. However, we propose integrating a sparse inversion into the iterative Marchenko scheme rather than Haindl's direct inversion method. The iterative framework was also applied to IJsseldijk and Wapenaar's work, which deals with the other situation [28]. As a result of this, our paper works towards a methodology to take care of the data that are subsampled in both source and receiver dimensions in the Marchenko method. This paper is organized as follows. First, we introduce the discrete representations for the Marchenko method and the problem of this method caused by irregular sampling. Subsequently, we integrate sparse inversion into the iterative Marchenko scheme and give the workflow of our method. Finally, numerical examples verify the performance of our method. The results show that this method effectively reconstructs obtained focusing functions and Green's functions in the Marchenko method under imperfect sampling.

2. Methods

2.1. Discrete Representations for the Marchenko Method

We assume an inhomogeneous lossless acoustic medium. The reflection response of the surface of this medium is given by $R(\mathbf{x}_R, \mathbf{x}_S, t)$, where $\mathbf{x}_S$ is the position of the source, $\mathbf{x}_R$ is the position of the receiver, and t is the time. A focal point $\mathbf{x}_A$ is defined inside the medium. The downgoing and upgoing Green's functions from the surface $\mathbb{S}_0$ to this focal point are, respectively, expressed as $G^+(\mathbf{x}_A, \mathbf{x}_R, t)$ and $G^-(\mathbf{x}_A, \mathbf{x}_R, t)$. The coupled Marchenko equation and Green's functions can be connected using focusing functions as follows [16]:

$$G^{\pm}(\mathbf{x}_A, \mathbf{x}_R, t) \mp f_1^{\pm}(\mathbf{x}_R, \mathbf{x}_A, \mp t) = \mp \int_{\mathbb{S}_0} R(\mathbf{x}_R, \mathbf{x}_S, t) * f_1^{\mp}(\mathbf{x}_S, \mathbf{x}_A, \mp t) \mathrm{d}\mathbf{x}_S. \tag{1}$$

where $f_1^{\pm}(\mathbf{x}_R, \mathbf{x}_A, \mp t)$ is the defined focusing functions, and $\pm$ denotes downgoing $(+)$ and upgoing $(-)$ propagation. The asterisk indicates a temporal convolution. In practical application, the infinite integral on the right side of Equation (1) is approximated by the finite sum of available sources [27]:

$$\hat{G}^{\pm}(\mathbf{x}_A, \mathbf{x}_R, t) \mp \hat{f}_1^{\pm}(\mathbf{x}_R, \mathbf{x}_A, \mp t) = \mp \sum_i R\left(\mathbf{x}_R, \mathbf{x}_S^{(i)}, t\right) * f_1^{\mp}\left(\mathbf{x}_S^{(i)}, \mathbf{x}_A, \mp t\right) * S(t), \tag{2}$$

where i is the source position, and $S(t)$ is the source wavelet. The integration in Equation (1) is performed under the source dimension. Through the source-receiver reciprocity theorem, the equation can be rewritten into the form of integrating under the receiver dimension:

$$G^{\pm}(\mathbf{x}_A, \mathbf{x}_S, t) \mp f_1^{\pm}(\mathbf{x}_S, \mathbf{x}_A, \mp t) = \mp \int_{\mathbb{S}_0} R(\mathbf{x}_R, \mathbf{x}_S, t) * f_1^{\mp}(\mathbf{x}_R, \mathbf{x}_A, \mp t) \mathrm{d}\mathbf{x}_R. \tag{3}$$

Therefore, Equation (2) is correspondingly modified as follows:

$$\hat{G}^{\pm}(\mathbf{x}_A, \mathbf{x}_S, t) \mp \hat{f}_1^{\pm}(\mathbf{x}_S, \mathbf{x}_A, \mp t) = \mp \sum_i R\left(\mathbf{x}_R^{(i)}, \mathbf{x}_S, t\right) * f_1^{\mp}\left(\mathbf{x}_R^{(i)}, \mathbf{x}_A, \mp t\right) * S(t). \tag{4}$$

Next, we consider the influence of incomplete acquisition geometry. For the sake of simplicity, here we only discuss the case of integrating under the receiver dimension (as mentioned above, this can be reciprocated with the case of integrating under the source dimension). Now, we rewrite Equation (4) as follows:

$$\begin{aligned} \hat{G}^{\pm}(\mathbf{x}_A, \mathbf{x}_S, t) \mp \hat{f}_1^{\pm}(\mathbf{x}_S, \mathbf{x}_A, \mp t) = \\ \mp \Phi_S(\mathbf{x}_S) \sum_i \Phi_R\left(\mathbf{x}_R^{(i)}\right) R\left(\mathbf{x}_R^{(i)}, \mathbf{x}_S, t\right) * f_1^{\mp}\left(\mathbf{x}_R^{(i)}, \mathbf{x}_A, \mp t\right) * S(t). \end{aligned} \tag{5}$$

where Φ_S and Φ_R are the sampling matrices on the source and receiver sides, respectively. If the receiver sampling is irregular (with $\Phi_S = 1$) when acquiring reflection data, the sum on the right side will introduce waveform distortions to the focusing functions and Green's functions on the left side. On the other hand, if the source sampling is irregular (with $\Phi_R = 1$), there will be both waveform distortions and spatial gaps left in the obtained focusing functions and Green's functions [26]. More details about both situations are in the next section.

2.2. The Standard Marchenko Method with Irregular Sampling

Let us look at the velocity model shown in Figure 1. The reflection response is obtained using 201 co-located sources and receivers with 10 m spacing. The time sampling interval is 4 ms. The seismic wavelet is a Ricker wavelet at 20 Hz. The focal point is located at (x = 0 m, z = 950 m). Figure 2a,b show the sampling matrices Φ_S and Φ_R, representing sampling masks for the source and receiver dimensions, respectively, with 40% of them randomly removed.

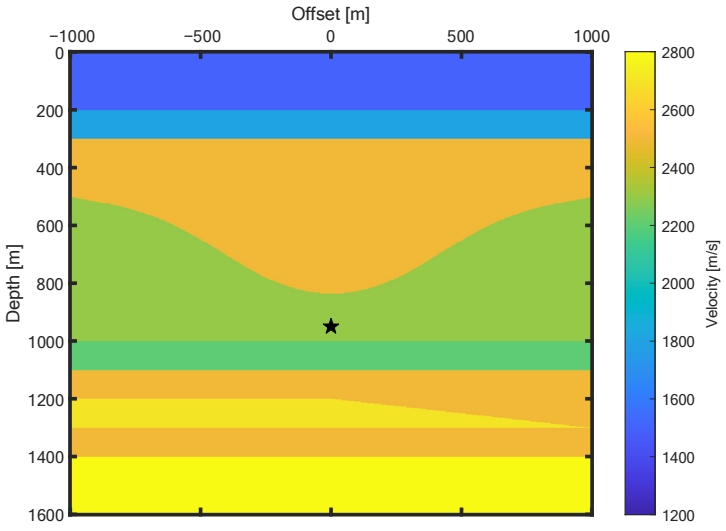

Figure 1. The velocity model. The black star indicates the position of the focal point at (x, z) = (0 m, 950 m).

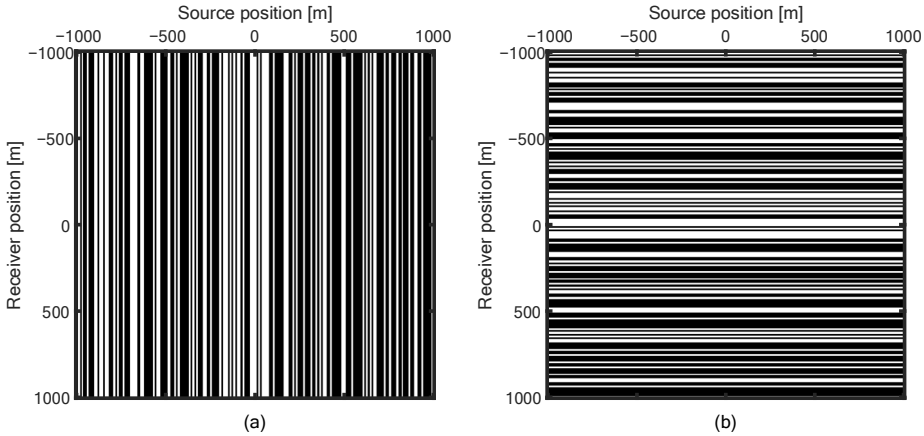

Figure 2. The sampling matrices. (**a**) is Φ_S (under the source dimension), and (**b**) is Φ_R (under the receiver dimension).

The standard Marchenko method is processed according to Equation (4). Figure 3a shows the focusing function with an irregular sampling of the sources and regular sampling of the receivers (i.e., $\Phi_S \neq 1$, $\Phi_R = 1$). Figure 4a is the corresponding Green's function. Figure 3b shows the focusing function with an irregular sampling of the receivers and regular sampling of the sources (i.e., $\Phi_S = 1$, $\Phi_R \neq 1$), and Figure 4b is the corresponding Green's function. As references, Figure 3c is the focusing function under regular sampling (i.e., with $\Phi_S \& \Phi_R = 1$), and Figure 4c is the subsequent Green's function. It should be noted that all the figures of focusing functions and Green's functions we show in this paper are the superposition of the upgoing and downgoing ones.

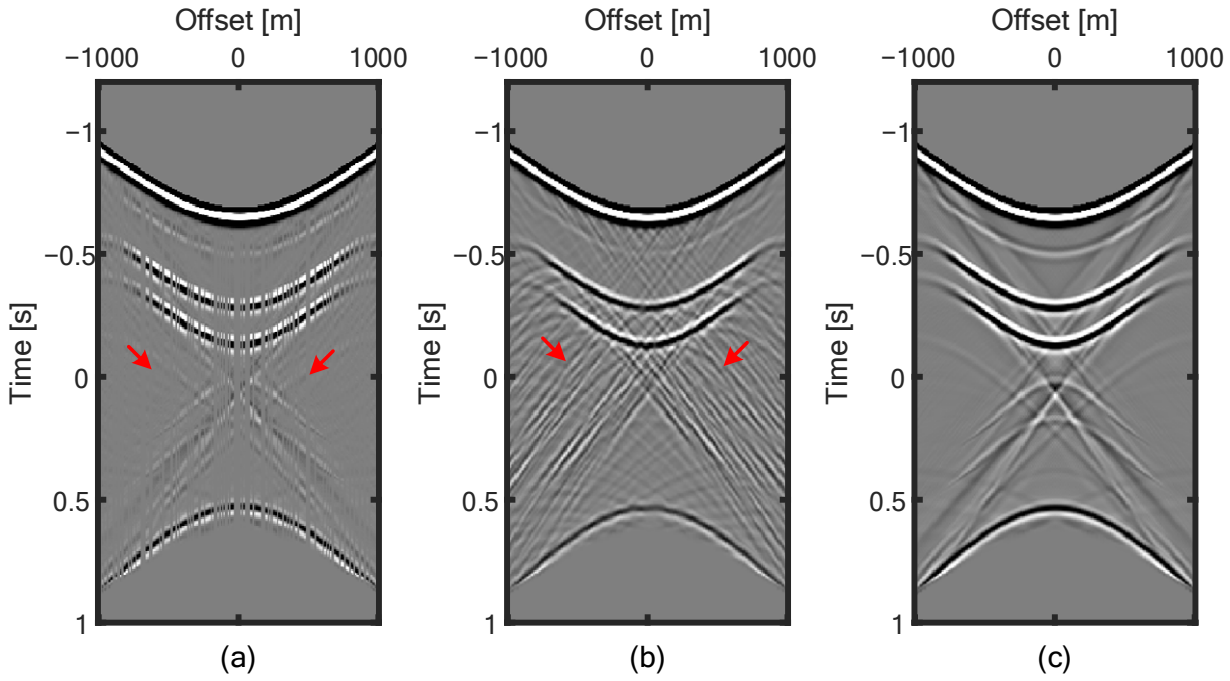

Figure 3. The focusing functions obtained by the standard Marchenko method integrated under the receiver dimension. They are sampled (**a**) under the source dimension; (**b**) under the receiver dimension; (**c**) regularly. Red arrows point out partial artifacts.

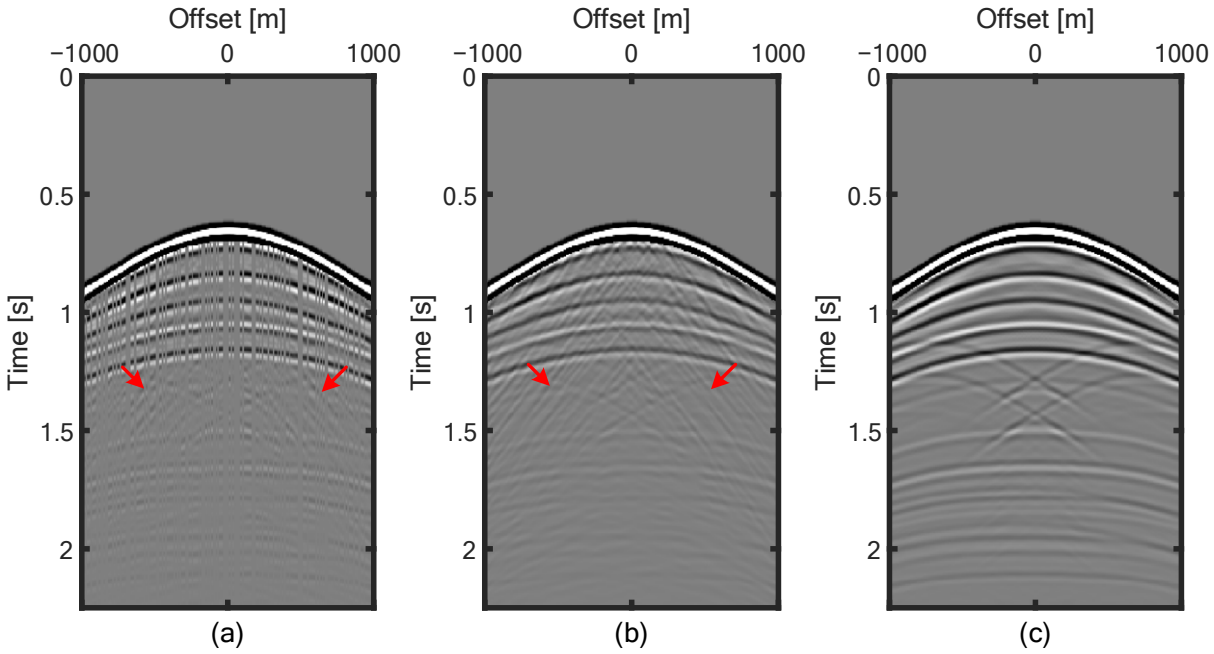

Figure 4. The Green's functions obtained using the standard Marchenko method integrated under the receiver dimension. They are sampled (**a**) under the source dimension; (**b**) under the receiver dimension; (**c**) regularly. Red arrows point out partial artifacts.

In Figures 3a and 4a, we can see that the focusing function and Green's function obtained by sampling and integrating under the different dimensions have clear space gaps and artifacts (partially pointed by red arrows). Furthermore, in Figures 3b and 4b, the focusing function and Green's function obtained using sampling and integrating under the same dimension have no gap in space, but artifacts do appear (partially pointed by red arrows).

This is because when the sampling is carried out under the source dimension, all the obtained reflection data R during acquisition have spatial gaps, which affect the spatial gaps in obtained focusing functions. In the subsequent iterations, the gaps in focusing functions enter the summation process [26]. On the other hand, when the sampling is under the receiver dimension, a part of R is missing due to Φ_R. In the summation process, the missing parts will cause artifacts. However, the non-zero elements still maintain good spatial sampling, which will not lead to spatial gaps. After the end of the iteration, the obtained focusing functions are substituted into Equation (4) to estimate Green's functions. So, the inaccuracy of focusing functions leads to the inaccuracy of the subsequent Green's functions.

2.3. Sparse Reconstruction of Focusing Functions

Our work focuses on the case of source subsampling, so we only consider the situation where $\Phi_S \neq 1$ and $\Phi_R = 1$ in Equation (5). In the rest of this paper, we replace Φ_S with Φ to represent irregular sampling for convenience. We now introduce sparse inversion theory.

In Compressive Sensing, wavefield reconstruction is achieved through sparse transformation and/or the inversion calculator with sparsity constraints [30]. Focusing functions are composed of mostly continuous events and can be traced in a time-offset plot, so they have many common features with other seismic wavefields. Haindl et al. showed that sparse transformation used for the wavefield reconstruction could also be used for the reconstruction of focusing functions [29]. Since our goal is to solve a redatuming problem with irregularly sampled input data (i.e., reflection response), we now turn to deal with the sparse reconstruction of focusing functions using reflection data with random gaps. Here,

we give only the formula derivation; please refer to the work of Haindl et al. for a detailed numerical demonstration.

We record the vector forms of the complete reflection response and the focusing function as $\boldsymbol{r}$ and $\boldsymbol{f}$, respectively, then the vector form of the missing reflection response is

$$\hat{\boldsymbol{r}} = \Phi \boldsymbol{r}, \tag{6}$$

where $\boldsymbol{r} \in \boldsymbol{R}^N$, $\hat{\boldsymbol{r}} \in \boldsymbol{R}^M$, $N > M$. $\Phi \in \boldsymbol{R}^{M \times N}$ is the sampling matrix. $\hat{\boldsymbol{r}}$ will also cause gaps in the follow-up focusing function, which is expressed as $\hat{\boldsymbol{f}}$. It follows

$$\hat{\boldsymbol{f}} = \Phi \boldsymbol{f}. \tag{7}$$

Assuming that $\boldsymbol{f}$ can be represented sparsely in the transform domain, the transform domain is called the sparse domain. Then we have

$$\boldsymbol{a} = \Psi \boldsymbol{f}, \tag{8}$$

where Ψ is the sparse basis, and $\boldsymbol{a}$ is the sparse coefficient of $\boldsymbol{f}$ in the sparse domain. Substitute Equation (8) into Equation (7), and we get

$$\hat{\boldsymbol{f}} = \Theta \boldsymbol{a}, \tag{9}$$

where $\Theta = \Phi \Psi^{-1}$. Ψ^{-1} is the inverse of Ψ. Θ is usually called recovery matrix. Since $N > M$, Equation (9) is underdetermined and has infinitely many solutions, so it is impossible to reconstruct the complete focusing function. However, we can obtain a unique solution if the recovery matrix Θ satisfies the Restricted Isometry Property (RIP) [31,32]. When the sampling matrix Φ is incoherent with the sparse basis Ψ, this property can be satisfied. Therefore, to reconstruct the complete focusing function, the direct way is to solve the L0-norm through continuous optimization:

$$\tilde{\boldsymbol{a}} = \underset{\boldsymbol{a}}{\operatorname{argmin}} \|\boldsymbol{a}\|_0 \quad s.t. \left\| \Theta \boldsymbol{a} - \hat{\boldsymbol{f}} \right\|_2 \leq \sigma, \tag{10}$$

where $\tilde{\boldsymbol{a}}$ is the optimal sparse coefficient, σ is the reconstruction error, and the constraint condition $\left\| \Theta \boldsymbol{a} - \hat{\boldsymbol{f}} \right\|_2 \leq \sigma$ ensures that the solution converges to the true value. Equation (10) is an underdetermined ill-posed problem. It is difficult to obtain an accurate solution. However, L0-norm and L1-norm can get the same approximate solution under a certain condition [33], so Equation (10) is transformed into a convex optimization problem:

$$\tilde{\boldsymbol{a}} = \underset{\boldsymbol{a}}{\operatorname{argmin}} \|\boldsymbol{a}\|_1 \quad s.t. \left\| \Theta \boldsymbol{a} - \hat{\boldsymbol{f}} \right\|_2 \leq \sigma, \tag{11}$$

Then the reconstructed focusing function can be obtained by

$$\tilde{\boldsymbol{f}} = \Psi^{-1} \tilde{\boldsymbol{a}}. \tag{12}$$

2.4. Sparse Inversion in Iterative Marchenko Scheme

We propose the workflow (Figure 5) referring to the frame of IJsseldijk and Wapenaar's work [28]. Our method reconstructs focusing functions in each iteration. The first step is to estimate the initial downgoing focusing function $f_{1,0}^{+}$ to start the iteration. To facilitate calculation, it is usually approximated by the time reversal of the direct arrival of Green's function G_d [34]:

$$f_{1,0}^{+}(\mathbf{x}_R, \mathbf{x}_A, t) \approx G_d(\mathbf{x}_R, \mathbf{x}_A, -t). \tag{13}$$

This approximation mainly means that the transmission losses at the interfaces are ignored. Equation (13) corresponds to step 1 in Figure 5.

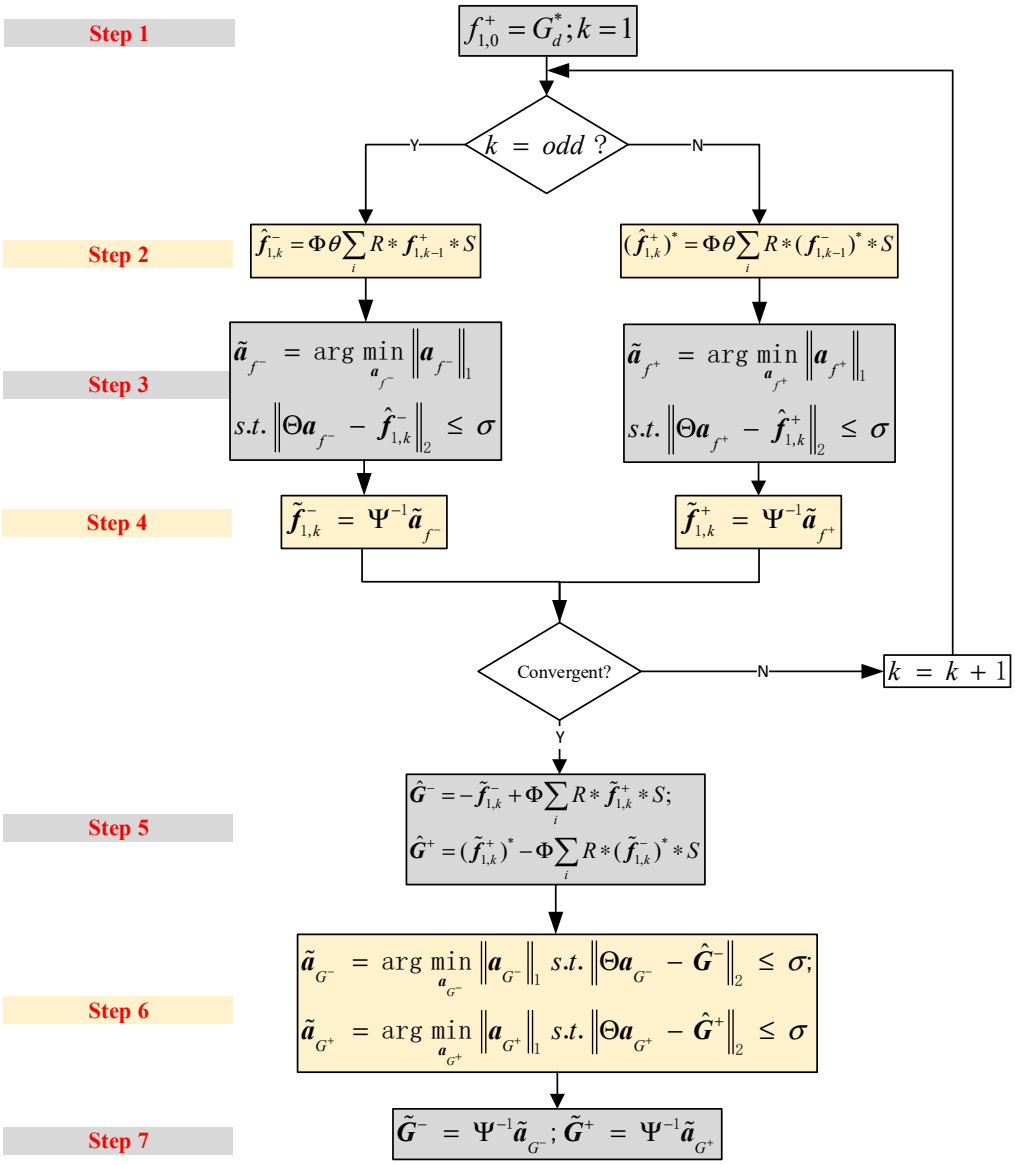

Figure 5. Workflow of the proposed Marchenko method. The focusing functions and Green's functions are recovered by Steps 3, 4, 6, and 7. S is the source signal, k is the number of iterations, the superscript asterisk is the time reversal, the internal asterisk is the convolution or correlation, Φ is the sampling matrix, and θ is the time window operator.

Next, the focusing functions are calculated according to Equation (4). The downgoing focusing function is retrieved from the initial condition of the first iteration or from the upgoing focusing function that is cross-correlated with the reflection response in the last iteration; the upgoing focusing function is the convolution of the downgoing focusing function and the reflection response. We use a time windowing operator θ to separate focusing functions from Green's functions. θ removes all energy whose arrival time is greater than or equal to the direct arrival time. This paragraph corresponds to step 2 in Figure 5.

In steps 3 and 4, we reconstruct $\hat{f}^{\pm}_{1,k}$ in Equation (5) by introducing sparse inversion. According to Equations (11) and (12), the reconstruction problem can be expressed as follows:

$$\tilde{a}_{f^{\pm}} = \underset{a_{f^{\pm}}}{\operatorname{argmin}} \left\| a_{f^{\pm}} \right\|_1 \quad s.t. \left\| \Theta a_{f^{\pm}} - \hat{f}^{\pm}_{1,k} \right\|_2 \leq \sigma, \tag{14}$$

and

$$\tilde{f}^{\pm}_{1,k} = \Psi^{-1} \tilde{a}_{f^{\pm}}. \tag{15}$$

Now we have the convergent and reconstructed focusing functions $\tilde{f}^{\pm}_{1,k}$. In step 5, we substitute $\tilde{f}^{\pm}_{1,k}$ into Equation (5) as follows:

$$\begin{aligned} \hat{G}^{\pm}(\mathbf{x}_A, \mathbf{x}_S, t) = \\ \pm \tilde{f}^{\pm}_{1,k}(\mathbf{x}_S, \mathbf{x}_A, \mp t) \mp \Phi \sum_i R\left(\mathbf{x}^{(i)}_R, \mathbf{x}_S, t\right) * \tilde{f}^{\mp}_{1,k}\left(\mathbf{x}^{(i)}_R, \mathbf{x}_A, \mp t\right) * S(t). \end{aligned} \tag{16}$$

Steps 6 and 7 are similar to steps 4 and 5. We reconstruct Green's functions through the following two equations:

$$\tilde{a}_{G^{\pm}} = \underset{a_{G^{\pm}}}{\operatorname{argmin}} \| a_{G^{\pm}} \|_1 \quad s.t. \left\| \Theta a_{G^{\pm}} - \hat{G}^{\pm} \right\|_2 \leq \sigma, \tag{17}$$

and

$$\tilde{G}^{\pm} = \Psi^{-1} \tilde{a}_{G^{\pm}}, \tag{18}$$

where $\tilde{G}^{\pm}$ are the recovered Green's functions. Equations (14)–(18) are the iterative Marchenko scheme with sparse inversion proposed in this paper.

3. Numeral Examples

The performance of our method is tested on the synthetic data. This test uses the same two-dimensional model as above (Figure 1), and the model parameters are also consistent with Section 2.2. For irregular sampling, 40% of the sources are randomly removed; the sampling mask is shown in Figure 2a. The direct arrival of Green's function between the depth of the source and the surface is estimated in the smooth model. As previously mentioned, the time reversal of direct arrival is used for the initial estimation of the downgoing focusing function. The reflection response and the initial estimate are the inputs required for the iterative Marchenko scheme. For the third and sixth steps of our method, we need to know the locations of the missing sources.

We use the SPGL1 solver [35,36] to invert Equations (15) and (18) in the Fourier transform, wavelet transform, and curvelet transform. Figure 6 compares the convergence in these domains. It can be seen that the results of sparse reconstruction using the wavelet transform (red line), which converges after 50 iterations, are the worst, while the Fourier transform (blue line) converges gradually after 30 iterations. From the overall results and convergence, the best effect is with the curvelet transform (yellow line), which starts to converge after 100 iterations. This shows that the focusing function is particularly sparse in the curvelet domain because the SPGL1 solver gradually loosens the sparsity constraint to facilitate smaller mismatches. Figure 7 shows the reconstructed focusing functions of the 100th iteration obtained by these three transforms. It can be clearly seen that the focusing function reconstructed with the curvelet transform (Figure 7d) is the most similar to the reference figure (Figure 7e). Figure 8 is the corresponding Green's functions. We can see that the curvelet domain (Figure 8d) makes the best reconstruction compared to the other domains.

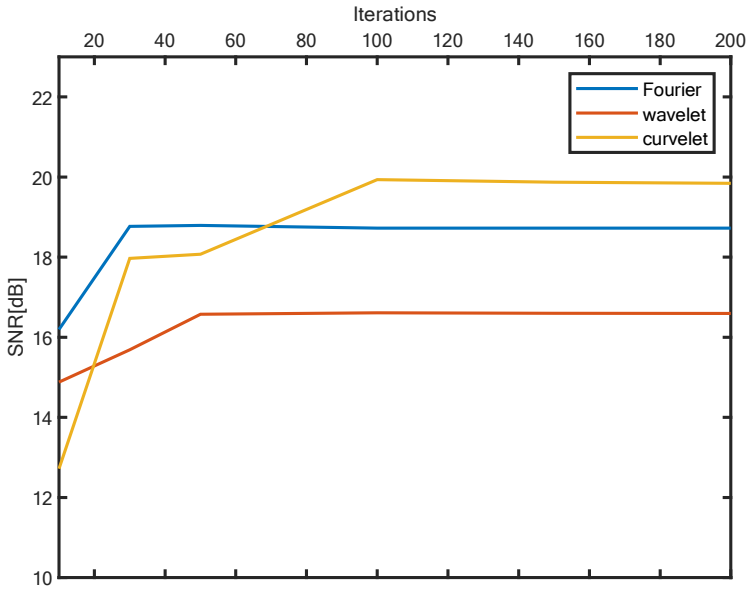

Figure 6. Comparison of convergence of SPGL1 algorithm in the sparse reconstruction of focusing functions, in which the red line is wavelet transform, the blue line is Fourier transform, and the yellow line is curvelet transform.

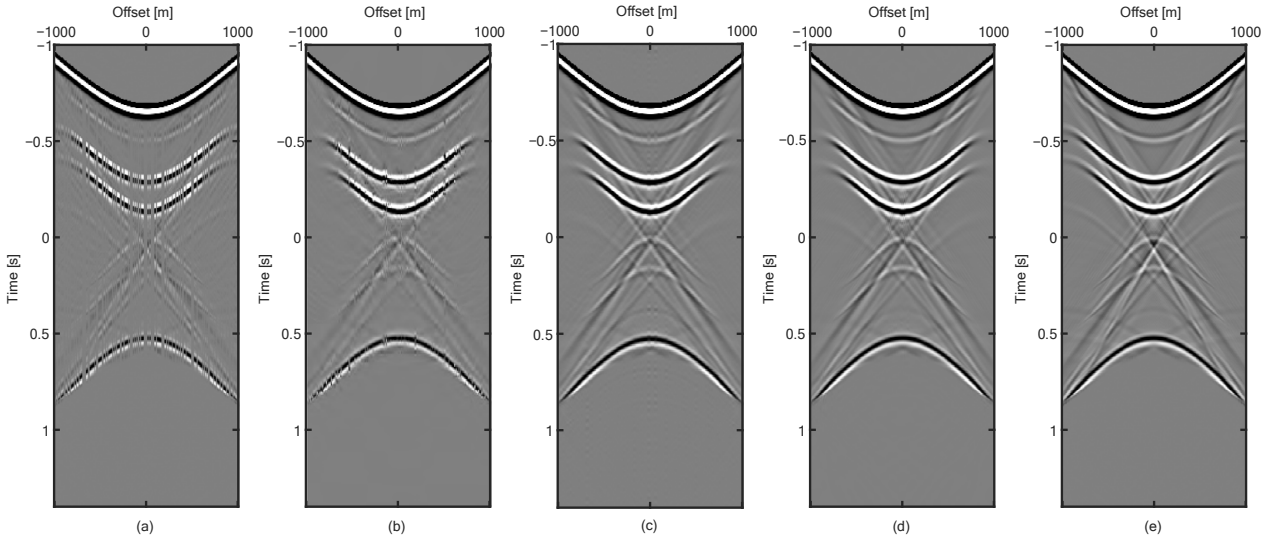

Figure 7. Comparison of focusing functions of the 100th iteration. (**a**) The focusing function without reconstruction, calculated by irregular sampling over the source dimension and integrating over the receiver dimension; (**b**) The reconstructed focusing function for sparse reconstruction in the wavelet domain; (**c**) The reconstructed focusing function for sparse reconstruction in Fourier domain; (**d**) The reconstructed focusing function for sparse reconstruction in curvelet domain; (**e**) The focusing function for reference.

After determining that the curvelet domain is the best transform domain in our method, we use the FISTA sparse solver [37] to invert Equations (14) and (17) as well. Figure 9 shows the convergence of the SPGL1 solver and the FISTA solver with curvelet transform. It can be seen that the FISTA solver (purple line) becomes flat after nearly 50 iterations, and the result of the 50th iteration is very close to that of the 100th iteration of the SPGL1 solver (yellow line). It means that the SPGL1 solver needs more than 100 iterations to achieve better results than the FISTA solver. We compare the focusing functions and final Green's functions obtained by the standard Marchenko method and our method in Figures 10 and 11. Figures 10b and 11b are reconstructed using our method

with the SPGL1 solver, and Figures 10c and 11c are with the FISTA solver. Compared with the reference Figures 10d and 11d, it can be seen that the gaps caused in the standard Marchenko method (Figures 10a and 11a) are effectively filled in our method with both solvers. To facilitate observation, in Figure 12, we enlarge the single traces of the four Green's functions in Figure 10, which are represented by blue, red, yellow, and purple lines, respectively. We can see that at x = 10 m (Figure 12a), the yellow line (FISTA solver) and purple line (reference) are well matched. At x = −960 m (Figure 12b), both red (SPGL1 solver) and yellow lines are matched with the purple line. Hence, this result proves the effectiveness of our reconstruction method, and our method with the FISTA solver is better than that with the SPGL1 solver at the near offset.

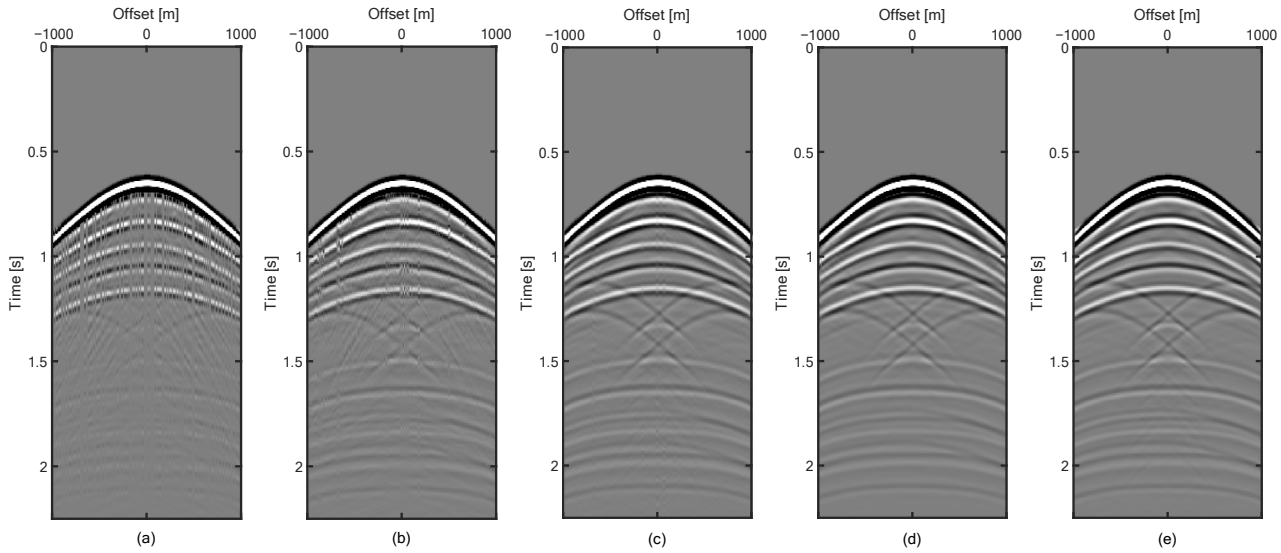

Figure 8. Comparison of Green's functions according to Figure 7. (**a**) Green's function without reconstruction calculated by irregular sampling over the source dimension and integrating over the receiver dimension; (**b**) Reconstruction in wavelet domain; (**c**) Reconstruction in Fourier domain; (**d**) Reconstruction in curvelet domain; (**e**) Green's function for reference.

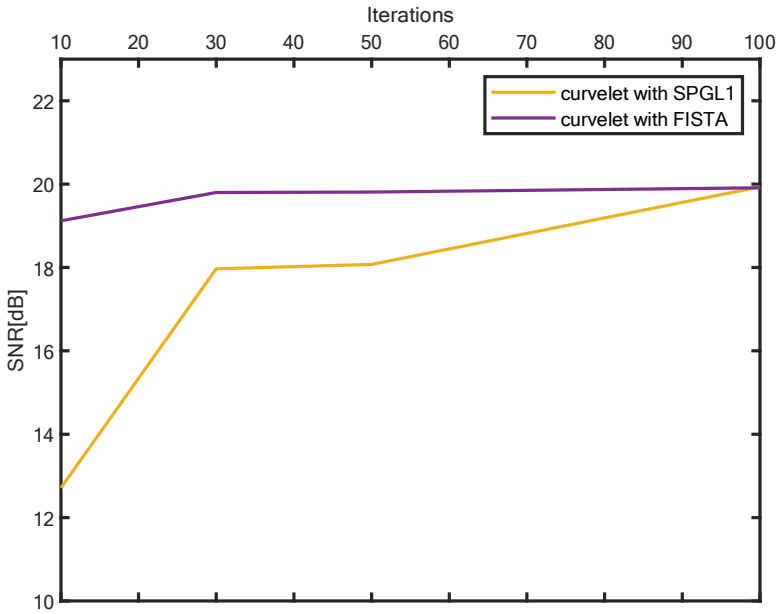

Figure 9. Comparison of convergence of the SPGL1 solver (yellow line) and the FISTA solver (purple line) in curvelet transform for focusing function reconstruction.

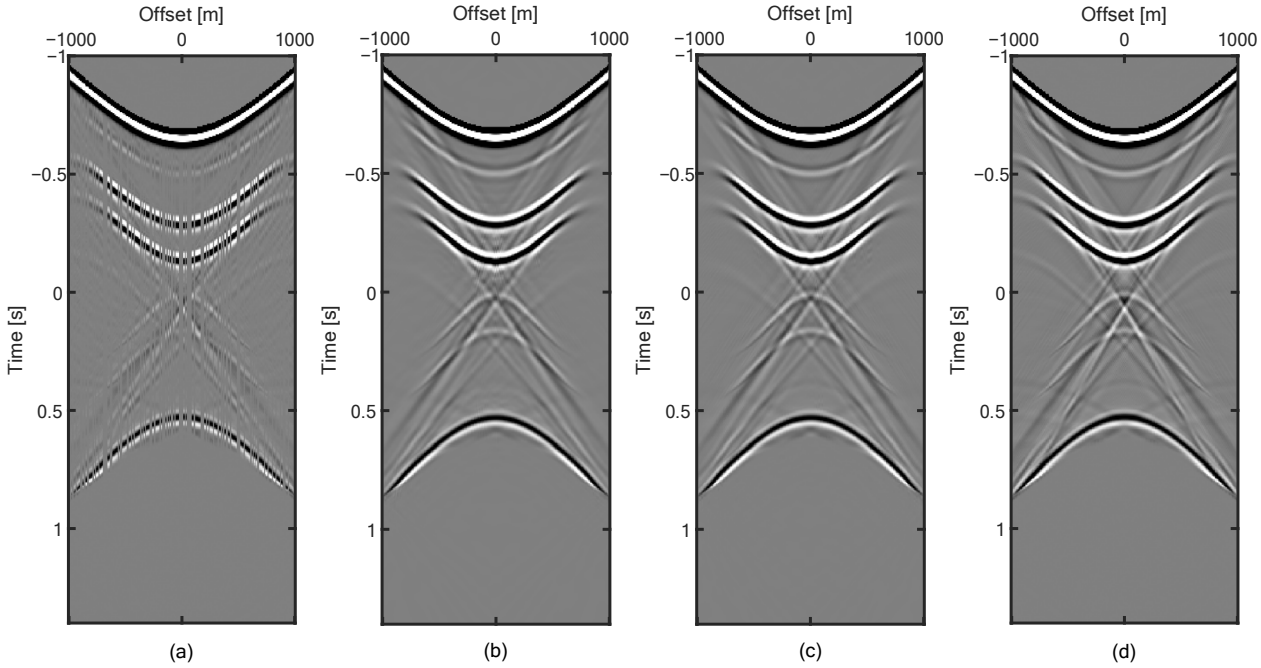

Figure 10. Comparison of the focusing functions. (**a**) is obtained using the standard Marchenko method with irregular sampling; (**b**) is obtained using sparse reconstruction with SPGL1 solver; (**c**) is obtained using sparse reconstruction with FISTA solver; and (**d**) is the reference focusing function.

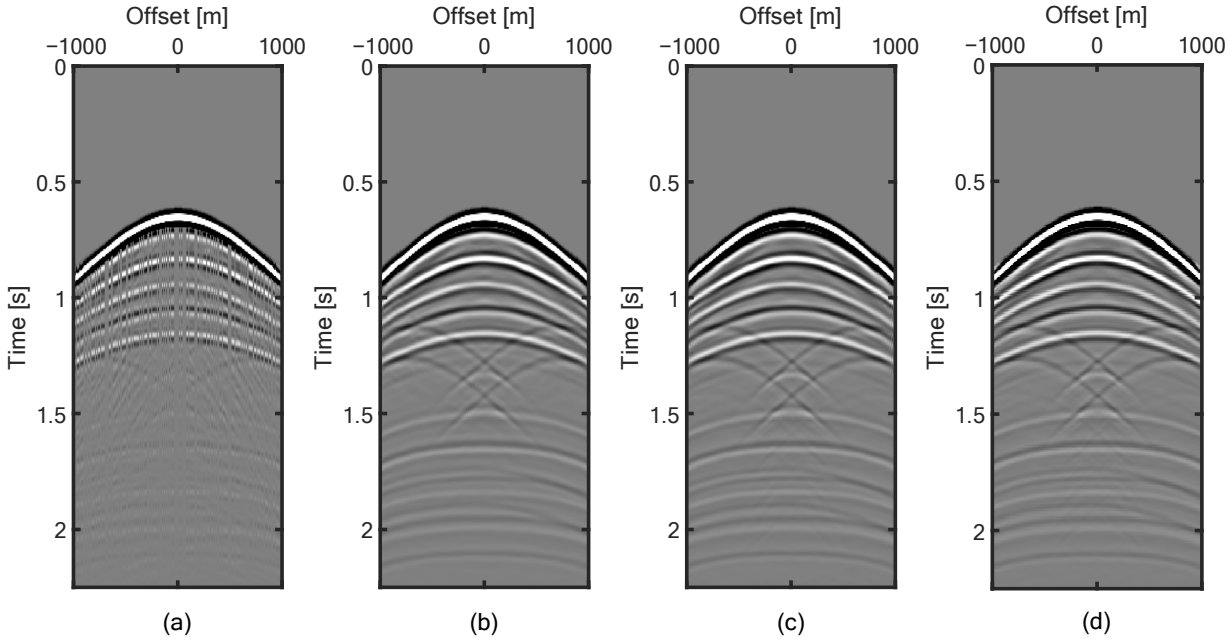

Figure 11. Comparison of Green's functions. (**a**) is obtained using the standard Marchenko method with irregular sampling; (**b**) is obtained using sparse reconstruction with SPGL1 solver; (**c**) is obtained using sparse reconstruction with FISTA solver, and (**d**) is the reference Green's function.

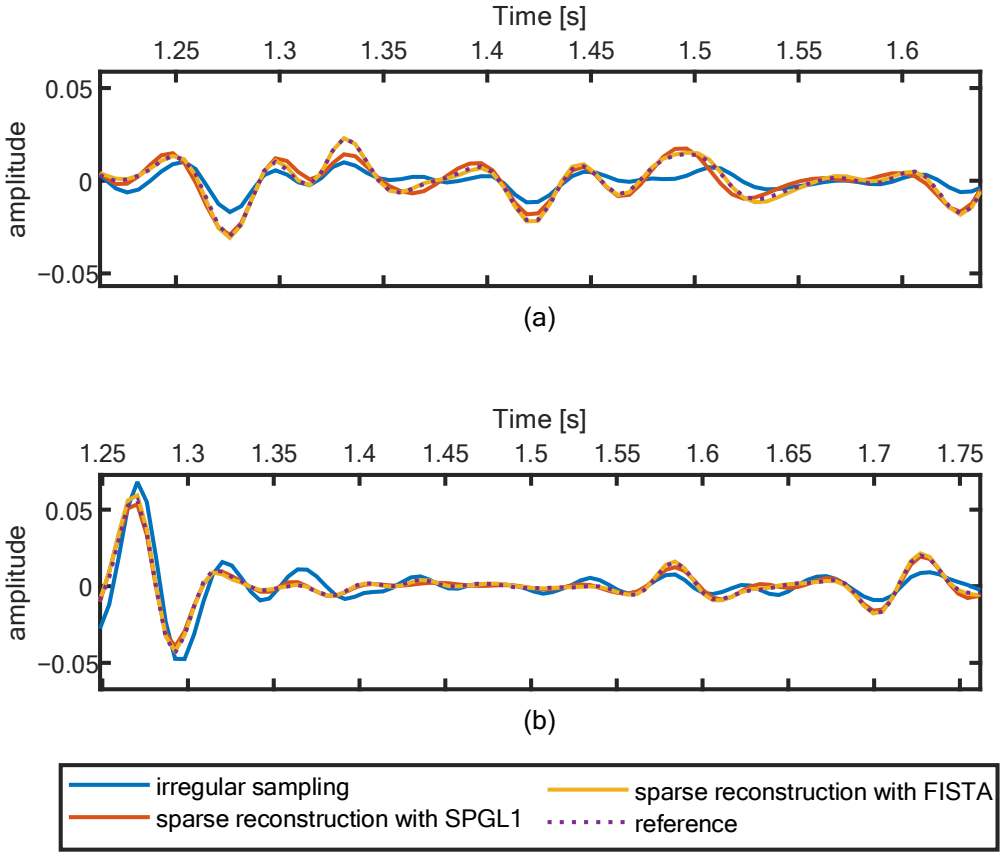

Figure 12. To compare the amplified traces of the Green's functions of Figure 10a–d, which are blue, red, yellow, and purple, respectively. They are at (**a**) near offset x = 10 m and (**b**) far offset x = −960 m.

4. Discussion

When the Marchenko method is used for seismic data sets with gaps in the acquisition geometry, sparse reconstruction for wavefields can also be used as a preprocessing process. Haindl's work [29] points out that the results obtained by taking sparse wavefield reconstruction as a preprocessing step are better than those obtained by combining sparse inversion with direct inversion of the Marchenko equations. However, preprocessing requires sparse reconstruction of all shots, which has a higher computational cost.

Some papers have already combined the Marchenko method with sparse inversion to deal with irregular sampling and integration in different dimensions [29,38,39]. For example, as mentioned in the Introduction section, Haindl et al. dealt with matrix Φ_S (with $\Phi_R = 1$) in a case where the focusing functions $\hat{f}_1^{\pm}$ were directly inverted from the Marchenko equation. However, their methods needed to directly invert the Marchenko equations. This means that when the amount of data is large, the inverse of the matrix in the inversion is difficult to solve. Our work also aims to handle this situation but is in the iterative Marchenko framework. Van IJsseldijk and Wapenaar's work also used the iterative scheme [28], but what they dealt with was Φ_R (with $\Phi_S = 1$). In our work, we show that Φ_S can also be dealt with in a case where $\hat{f}_1^{\pm}$ are found by the iterative scheme. A logical next step may be to combine this with the work of IJsseldijk and Wapenaar to deal with both Φ_S and Φ_R.

5. Conclusions

One limitation of the standard Marchenko method is the need for well-sampled and collocated sources and receivers. This paper broadens this requirement and proves that the obtained focusing functions and Green's functions can be improved by sparse inversion

when there are randomly distributed gaps in the input of the Marchenko method. We solve the problem of gaps and artifacts between the focusing functions and Green's function caused by irregular source sampling. For this method, we need to know the locations of the missing sources. We extend four steps (Steps 3, 4, 6, and 7) in each iteration of the standard Marchenko method. Our work casts the ideas of Haindl et al. into the framework of IJsseldijk and Wapenaar's work. We pose a step to simultaneously deal with two cases of sampling and integration in the same and different dimensions.

Author Contributions: Conceptualization, J.Z. and L.H.; methodology, J.Z.; software, J.Z.; validation, J.Z.; writing—original draft preparation, J.Z.; writing—review and editing, J.Z. and L.H.; supervision, L.H.; project administration, L.H.; funding acquisition, L.H. All authors have read and agreed to the published version of the manuscript.

Funding: This research was funded by the National Natural Science Foundation of China, grant numbers 42074154 and 42130805.

Data Availability Statement: Not applicable.

Conflicts of Interest: The authors declare no conflict of interest.

References

1. Slob, E.; Wapenaar, K.; Broggini, F.; Snieder, R. Seismic reflector imaging using internal multiples with Marchenko-type equations. *Geophysics* **2014**, *79*, S63–S76. [CrossRef]
2. Wapenaar, K.; Thorbecke, J.; Van Der Neut, J.; Broggini, F.; Slob, E.; Snieder, R. Marchenko imaging. *Geophysics* **2014**, *79*, WA39–WA57. [CrossRef]
3. Wapenaar, K.; Brackenhoff, J.; Dukalski, M.; Meles, G.; Reinicke, C.; Slob, E.; Staring, M.; Thorbecke, J.; van der Neut, J.; Zhang, L. Marchenko redatuming, imaging, and multiple elimination and their mutual relations. *Geophysics* **2021**, *86*, WC117–WC140. [CrossRef]
4. Lomas, A. Subsurface Seismic Imaging in the Presence of Multiply Scattered Waves. Ph.D. Thesis, University of Edinburgh, Edinburgh, UK, 2019.
5. Marchenko, V.A. On reconstruction of the potential energy from phases of the scattered waves. *Dokl. Akad. Nauk. SSSR* **1955**, *104*, 695–698.
6. Agranovich, Z.S.; Marchenko, V.A. *The Inverse Problem of Scattering Theory*; Gordon and Breach: New York, NY, USA, 1963.
7. Burridge, R. The Gelfand-Levitan, the Marchenko, and the Gopinath-Sondhi integral equations of inverse scattering theory, regarded in the context of inverse impulse-response problems. *Wave Motion* **1980**, *2*, 305–323. [CrossRef]
8. Marchenko, V.A. *Nonlinear Equations and Operator Algebras*; Springer Science & Business Media: Berlin/Heidelberg, Germany, 1987.
9. Marchenko, V.; Slavin, V. *Inverse Problems in the Theory of Small Oscillations*; American Mathematical Society: Providence, RI, USA, 2018.
10. Chadan, K.; Sabatier, P.C. *Inverse Problems in Quantum Scattering Theory*; Springer Science & Business Media: Berlin/Heidelberg, Germany, 2012.
11. Broggini, F.; Snieder, R. Connection of scattering principles: A visual and mathematical tour. *Eur. J. Phys.* **2012**, *33*, 593. [CrossRef]
12. Bakulin, A.; Calvert, R. The virtual source method: Theory and case study. *Geophysics* **2006**, *71*, SI139–SI150. [CrossRef]
13. Curtis, A.; Gerstoft, P.; Sato, H.; Snieder, R.; Wapenaar, K. Seismic interferometry—Turning noise into signal. *Lead. Edge* **2006**, *25*, 1082–1092. [CrossRef]
14. Snieder, R.; Wapenaar, K.; Larner, K. Spurious multiples in seismic interferometry of primaries. *Geophysics* **2006**, *71*, SI111–SI124. [CrossRef]
15. Wapenaar, K.; Broggini, F.; Slob, E.; Snieder, R. Three-dimensional single-sided Marchenko inverse scattering, data-driven focusing, Green's function retrieval, and their mutual relations. *Phys. Rev. Lett.* **2013**, *110*, 084301. [CrossRef]
16. Wapenaar, K.; Slob, E. On the Marchenko equation for multicomponent single-sided reflection data. *Geophys. J. Int.* **2014**, *199*, 1367–1371. [CrossRef]
17. Reinicke Urruticoechea, C. Elastodynamic Marchenko Inverse Scattering: A Multiple-Elimination Strategy for Imaging of Elastodynamic Seismic Reflection Data. Ph.D. Thesis, Delft University of Technology, Delft, The Netherlands, 2020.
18. Singh, S.; Snieder, R.; Behura, J.; van der Neut, J.; Wapenaar, K.; Slob, E. Marchenko imaging: Imaging with primaries, internal multiples, and free-surface multiples. *Geophysics* **2015**, *80*, S165–S174. [CrossRef]
19. Slob, E. Green's function retrieval and Marchenko imaging in a dissipative acoustic medium. *Phys. Rev. Lett.* **2016**, *116*, 164301. [CrossRef] [PubMed]
20. Behura, J.; Wapenaar, K.; Snieder, R. Autofocus imaging: Image reconstruction based on inverse scattering theory. *Geophysics* **2014**, *79*, A19–A26. [CrossRef]
21. Van der Neut, J.; Wapenaar, K.; Thorbecke, J.; Slob, E.; Vasconcelos, I. An illustration of adaptive Marchenko imaging. *Lead. Edge* **2015**, *34*, 818–822. [CrossRef]

22. Meles, G.A.; Wapenaar, K.; Curtis, A. Reconstructing the primary reflections in seismic data by Marchenko redatuming and convolutional interferometry. *Geophysics* **2016**, *81*, Q15–Q26. [CrossRef]
23. Zhang, L.; Slob, E. Free-surface and internal multiple elimination in one step without adaptive subtractionMultiple elimination. *Geophysics* **2019**, *84*, A7–A11. [CrossRef]
24. Zhang, L.; Thorbecke, J.; Wapenaar, K.; Slob, E. Transmission compensated primary reflection retrieval in the data domain and consequences for imaging. *Geophysics* **2019**, *84*, Q27–Q36. [CrossRef]
25. Ravasi, M. Rayleigh-Marchenko redatuming for target-oriented, true-amplitude imaging. *Geophysics* **2017**, *82*, S439–S452. [CrossRef]
26. Peng, H.; Vasconcelos, I. A study of acquisition-related sub-sampling and aperture effects on Marchenko focusing and redatuming. In Proceedings of the SEG International Exposition and Annual Meeting, San Antonio, TX, USA, 15–20 September 2019.
27. Wapenaar, K.; van IJsseldijk, J. Discrete representations for Marchenko imaging of imperfectly sampled data. *Geophysics* **2020**, *85*, A1–A5. [CrossRef]
28. Van Ijsseldijk, J.; Wapenaar, K. Adaptation of the iterative Marchenko scheme for imperfectly sampled data. *Geophys. J. Int.* **2021**, *224*, 326–336. [CrossRef]
29. Haindl, C.; Ravasi, M.; Broggini, F. Handling gaps in acquisition geometries—Improving Marchenko-based imaging using sparsity-promoting inversion and joint inversion of time-lapse data. *Geophysics* **2021**, *86*, S143–S154. [CrossRef]
30. Hennenfent, G.; Herrmann, F.J. Simply denoise: Wavefield reconstruction via jittered undersampling. *Geophysics* **2008**, *73*, V19–V28. [CrossRef]
31. Baraniuk, R.G. Compressive sensing. *IEEE Signal Process. Mag.* **2007**, *24*, 118–121. [CrossRef]
32. Candes, E.J. The restricted isometry property and its implications for compressed sensing. *Comptes Rendus Math.* **2008**, *346*, 589–592. [CrossRef]
33. Donoho, D.L. Compressed sensing. *IEEE Trans. Inf. Theory* **2006**, *52*, 1289–1306. [CrossRef]
34. Thorbecke, J.; Slob, E.; Brackenhoff, J.; van der Neut, J.; Wapenaar, K. Implementation of the Marchenko method. *Geophysics* **2017**, *82*, WB29–WB45. [CrossRef]
35. Van den Berg, E.; Friedlander, M.P. SPGL1: A Solver for Large-Scale Sparse Reconstruction. 2007. Available online: https://friedlander.io/spgl1 (accessed on 28 November 2022).
36. Van den Berg, E.; Friedlander, M.P. Probing the Pareto frontier for basis pursuit solutions. *SIAM J. Sci. Comput.* **2008**, *31*, 890–912. [CrossRef]
37. Beck, A.; Teboulle, M. A fast iterative shrinkage-thresholding algorithm for linear inverse problems. *SIAM J. Imaging Sci.* **2009**, *2*, 183–202. [CrossRef]
38. Haindl, C.M.; Broggini, F.; Ravasi, M.; van Manen, D.J. Using sparsity to improve the accuracy of Marchenko imaging given imperfect acquisition geometries. In Proceedings of the 80th EAGE Conference and Exhibition, Copenhagen, Denmark, 10 June–15 July 2018; European Association of Geoscientists & Engineers: Houten, The Netherlands, 2018; Volume 2018, pp. 1–5.
39. Zhang, M. Compressive Sensing Acquisition with Application to Marchenko Imaging. *Pure Appl. Geophys.* **2022**, *179*, 2382–2404. [CrossRef]